Supporting Information

for

Influence of Charge Scaling on the Solvation Properties of Ionic Liquid Solutions

Kai Cui[1], Arun Yethiraj[1], and J. R. Schmidt[1,*]

[1]Theoretical Chemistry Institute and Department of Chemistry, University of Wisconsin-Madison, 1101 University Avenue, Madison, Wisconsin 53706, United States

[*]Corresponding Author, Email: schmidt@chem.wisc.edu

S1 Force Field Parameters

S1.1 Solute Atomic Charge Comparison

Atom	EPM2	SAPT	OPLS
CO_2-C	+0.6512	+0.65738	—
CO_2-O	-0.3256	-0.32869	—
NH_3-N	—	-1.0503	-1.02
NH_3-H	—	+0.3501	+0.34

Table S1: Compare atomic charge of solutes in different force fields.[1–4]

S1.2 NH_3 SAPT FF validation

Figure S1 shows the calculated second virial coefficient, B_2, of NH_3 using OPLS and two SAPT FF variants as compared to experimental. We find that the OPLS result (blue triangles) agrees well with the experiment, while the isotropic SAPT FF with Born-Meyer functional form (SAPT-original, filled red squares) exhibits overly strong dimer interaction; this deviation was previously shown to arise from atomic anisotropy in the intermolecular interaction, and could be corrected introducing atomic anisotropy..[5]

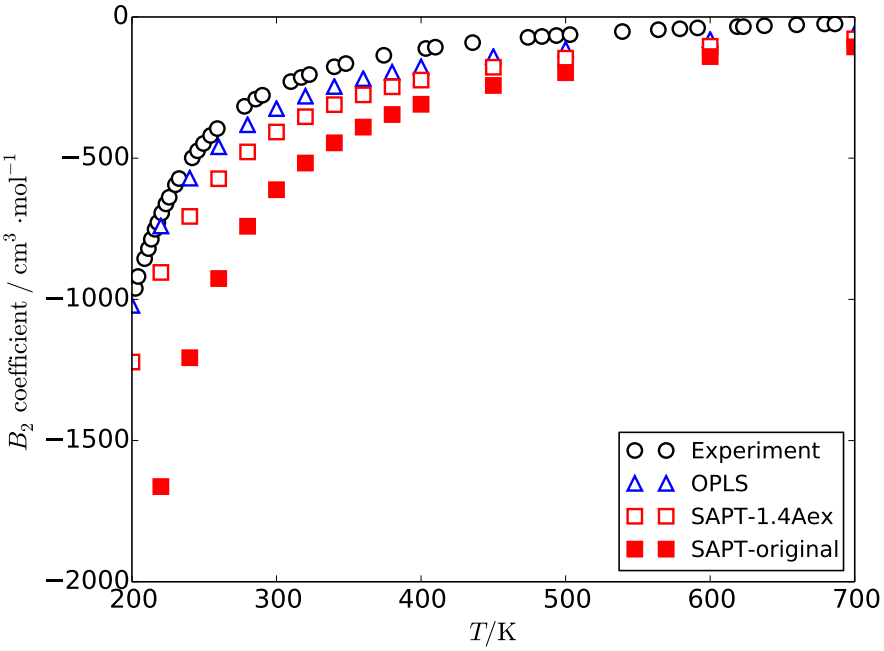

Figure S1: Calculated second virial coefficient B_2 of NH_3 compared to experimental values.[6]

Rather than utilize an anistropic form, we chose to increase the short-range repulsion by scaling the A_{exch} parameter by 1.4. The calculated B_2 resulting from this adjusted FF is shown as open red squares, yielding a

significant improvement in the calculated B_2. This adhoc fix influences only the exchange repulsion parameters and does not effect the electrostatic interaction. We use this optimized SAPT NH_3 FF for all subsequent solvation studies.

S2 Thermodynamic Integration Details

For OPLS-like (LJ + point charges) FFs, decoupling is separated into two steps: first lineally eliminate the Coulomb interaction by linearly scaling the atomic charge of the solute $q \to \lambda q$; then turn eliminate the LJ interaction using a soft-core potential to avoid the singularity of integrand at $\lambda = 0$:[7]

$$U_{\mathrm{LJ}}^{\lambda} = 4\lambda\varepsilon \left[\left(\frac{\sigma}{r_{\mathrm{eff}}} \right)^{12} - \left(\frac{\sigma}{r_{\mathrm{eff}}} \right)^{6} \right], \quad r_{\mathrm{eff}} = \sigma \left[0.5(1-\lambda) + \left(\frac{r}{\sigma} \right)^{6} \right]^{1/6} \tag{1}$$

For hard sphere (WCA) models we can use similar soft-core scheme to turn off the interaction:

$$U_{\mathrm{HS}}^{\lambda} = \begin{cases} 4\lambda\varepsilon \left[\left(\frac{\sigma}{r_{\mathrm{eff}}} \right)^{12} - \left(\frac{\sigma}{r_{\mathrm{eff}}} \right)^{6} \right] + \varepsilon & , \; r_{\mathrm{eff}} < 2^{\frac{1}{6}}\sigma \\ 0 & , \; r_{\mathrm{eff}} \geq 2^{\frac{1}{6}}\sigma \end{cases}, \quad r_{\mathrm{eff}} = \sigma \left[0.5(1-\lambda) + \left(\frac{r}{\sigma} \right)^{6} \right]^{1/6} \tag{2}$$

In the case of SAPT FF, the decoupling scheme is slightly more complex. For the electrostatic part, we use a linear scaling for both atomic and Drude charges, while also scaling the polarizability quadratically to avoid over-polarization. For the exp-n (exchange + dispersion), we here first convert the exp-n potential to a HS potential via a linear decoupling:

$$U_{\mathrm{exp-HS}}^{\lambda} = \lambda U_{\mathrm{exp-n}} + (1-\lambda) U_{\mathrm{HS}} \tag{3}$$

and then utilize a standard soft-core potential to achieve full decoupling.

For smooth electrostatic and the exp-n to HS conversion, 6 λ parameters (0, 0.2, 0.4, ... 1.0) were used; for LJ or HS case, 11 λ parameters (0, 0.1, 0.2, ..., 1.0) were used. We estimated the uncertainty of ΔG_{solv} by block averaging.[8]

S3 Neat IL properties

Properties	density ($g \cdot cm^{-3}$)	ΔH_{vap} ($kJ \cdot mol^{-1}$)	D_+ ($10^{-11}\, m^2 \cdot s^{-1}$)	D_- ($10^{-11}\, m^2 \cdot s^{-1}$)	η (cP)
SAPT	1.181	128	29.5 (400K)	27.1 (400K)	93
0.8*OPLS	1.150	140.5	43.1 (425K)	42.9 (425K)	97.8
Experiment	1.202	128, 136	27.5 (400K), 40.0 (425K)	31.6 (400K), 47.6 (425K)	90.4

Table S2: Comparison of the predictions of neat IL properties by SAPT and 0.8*OPLS.

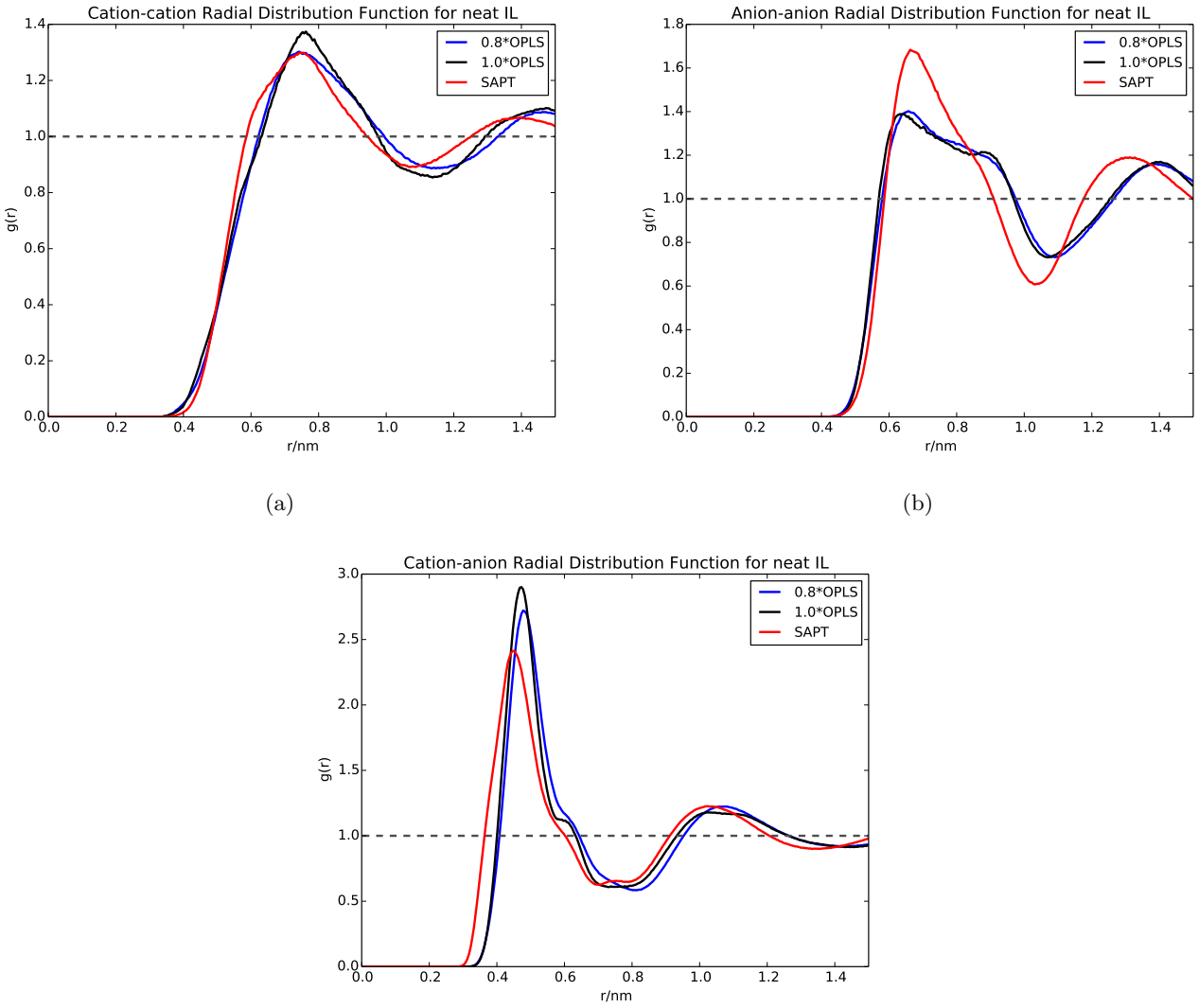

(a) (b)

(c)

Figure S2: Ion-ion RDF for neat [BMIM][BF_4] calculated by 0.8*OPLS and SAPT FF.

S4 Extrapolation of ΔH_{solv} for Real Systems

Because of the slow dynamics at room temperature, the enthalpy of solvation at room temperature was also obtained by extrapolating ΔH_{solv} calculated at elevated temperature (350, 400 and 450 K) back to low temperature. Assuming the heat capacity change of solvation, $\Delta C_{p,\mathrm{solv}}$, is independent of temperature, we can the temperature dependence of ΔH by:

$$\Delta H_{\mathrm{solv}}(T) = \Delta H_{\mathrm{solv}}(T=0) + \Delta C_{p,\mathrm{solv}} T \tag{4}$$

MD simulations were run at 350, 400 and 450K with the same settings as introduced in the main text. The fitted ΔH line is shown in Figure S3. The detailed enthalpy result as well as the electrostatic component at elevated temperatures are shown in Table S4. The $\Delta H - T$ plot shows fairly good linear behavior, indicating that the assumption that $\Delta C_{p,\mathrm{solv}}$ is independent on temperature is reasonable. The colored areas in Figure S3 represent the roughly estimated uncertainties of the fitted curve due to the uncertainty of each point. The extrapolated ΔH_{solv} values were listed in Table S3, which are consistent with those obtained via direct simulation.

$\Delta H_{\mathrm{extrapolate}}/\mathrm{kJ \cdot mol^{-1}}$	SAPT	0.8*OPLS
CO_2-[BMIM][BF_4]	-13.2 (-13.0)	-14.7 (-13.7)
NH_3-[BMIM][BF_4]	-25.3 (-25.7)	-17.4 (-17.1)

Table S3: Enthalpy of solvation of CO_2/NH_3-[BMIM][BF_4] system, extrapolated to 298K based on ΔH_{solv} values at elevated temperature. Numbers in the parentheses shows the brute force simulation results at 298K for comparison.

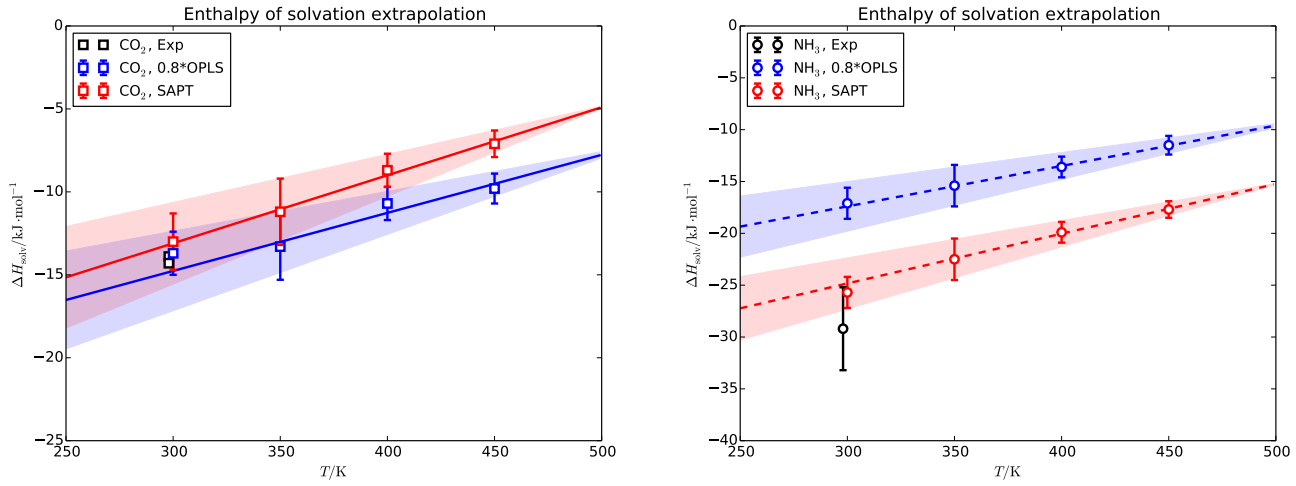

(a) (b)

Figure S3: Enthalpy of solvation of (a) CO_2-[BMIM][BF_4] and (b) NH_3-[BMIM][BF_4] system, extrapolated to room temperature. The squares and solid lines indicates the simulation ΔH values and fitted lines of CO_2 solution and the circles and dashed lines indicate those for NH_3 solution. The red markers and lines shows the result using SAPT FF, and the blue ones are results using 0.8*OPLS FF. Experimental ΔH values at 298 K are shown as black markers. The area filled by light color shows the roughly estimated uncertainty of the fitted lines.

T/K	CO_2-[BMIM][BF_4]		NH_3-[BMIM][BF_4]	
	SAPT	0.8*OPLS	SAPT	0.8*OPLS
ΔH_{solv}/kJ · mol^{-1}				
350	-11.2 ± 2.0	-13.3 ± 2.0	-22.5 ± 2.0	-15.4 ± 2.0
400	-8.7 ± 1.0	-10.7 ± 1.0	-19.9 ± 1.0	-13.6 ± 1.0
450	-7.1 ± 0.8	-9.8 ± 0.8	-17.7 ± 0.9	-11.5 ± 0.9
E_{elst}/kJ · mol^{-1}				
350	-10.6 ± 2.0	-8.3 ± 2.0	-40.7 ± 2.0	-26.5 ± 2.0
400	-9.3 ± 1.0	-7.9± 1.0	-38.7 ± 1.0	-24.6 ± 1.0
450	-7.8 ± 0.8	-6.8 ± 0.8	-35.4 ± 0.9	-22.7 ± 0.9

Table S4: Enthalpy of solvation and Electrostatic component of CO_2/NH_3-[BMIM][BF_4] interaction at elevated temperature.

S5 Radial Distribution Function for hard sphere model solutions

Solute-solvent site-site Radial distribution functions (RDF) of the hard sphere model solutions are calculated from the simulation trajectories. Since H atoms on cations and F atoms on anions are the atoms that have direct contact with the solute, we only show the solute-H and solute-F RDFs here, as in Figure S5−S6. The H atom labels on the cation are shown in Figure S4.

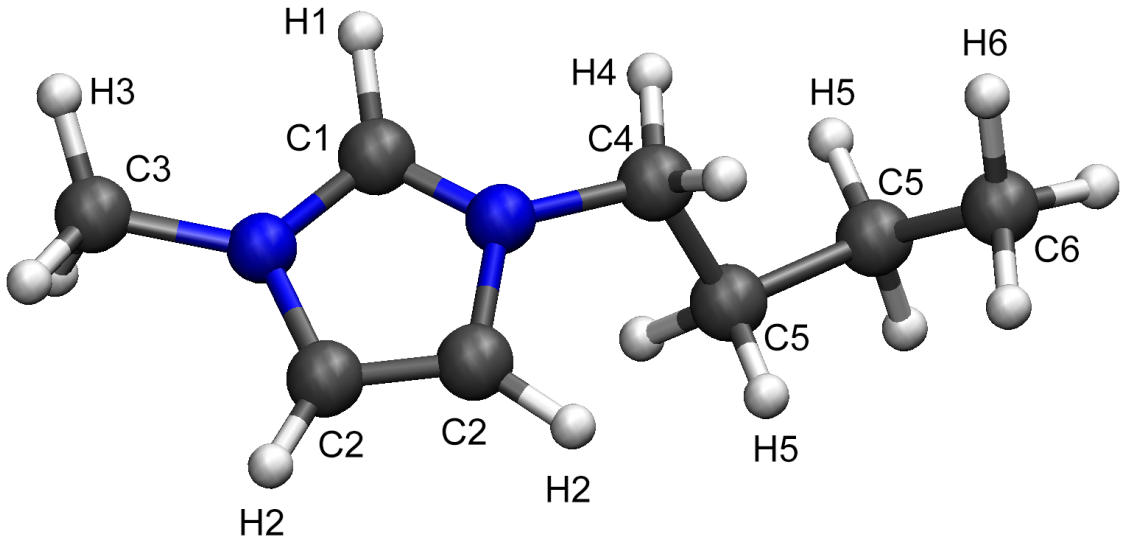

Figure S4: Atom labels for $[BMIM]^+$ cation.

S5.1 HS

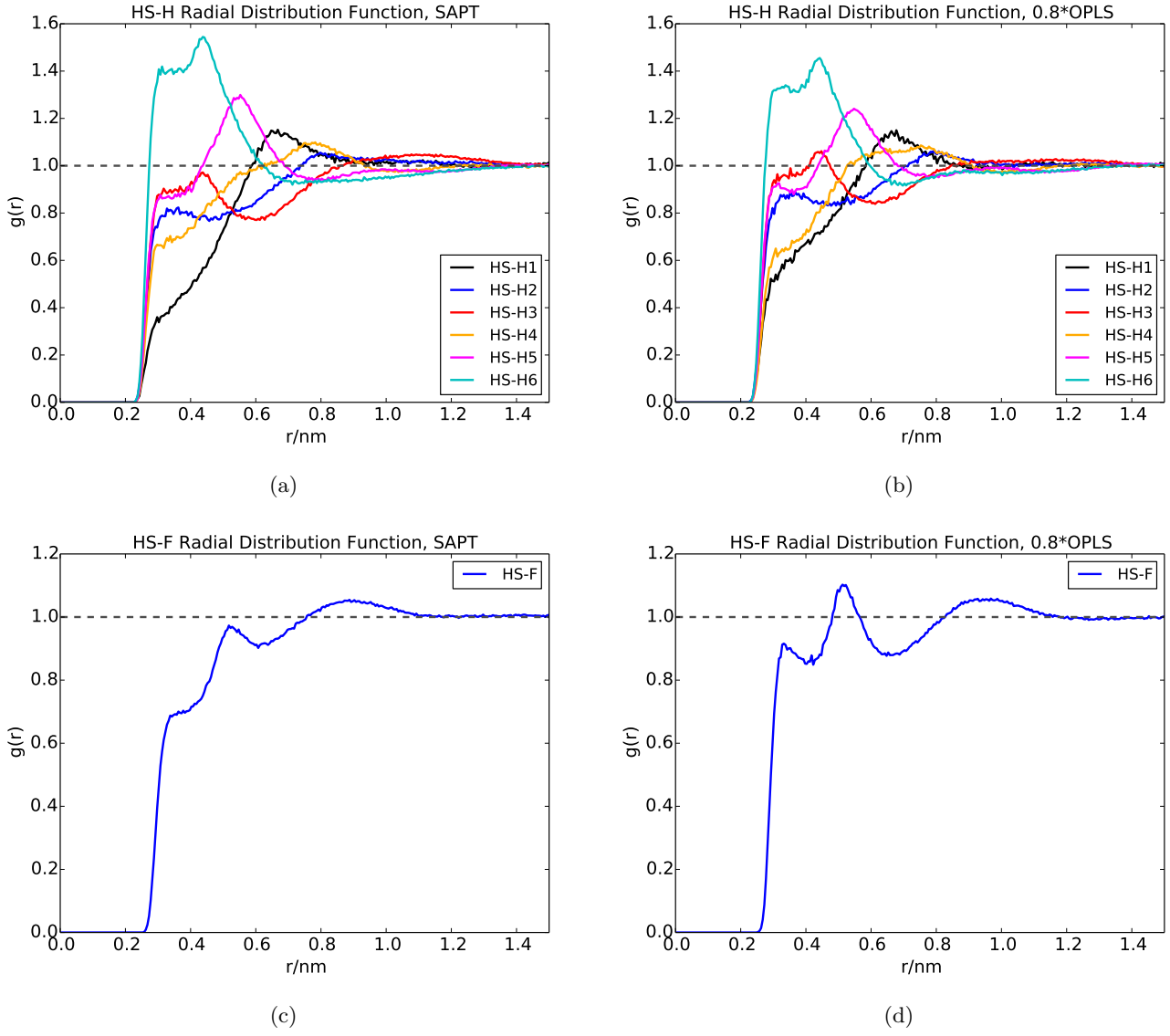

Figure S5: Comparing the 0.8*OPLS and SAPT FF solute-solvent site-site RDFs, HS case. (a) solute-H RDF for SAPT, (b) solute-H RDF for 0.8*OPLS, (c) solute-F RDF for SAPT, (d) solute-F RDF for 0.8*OPLS.

S5.2 polarHS, $q = 0.5$

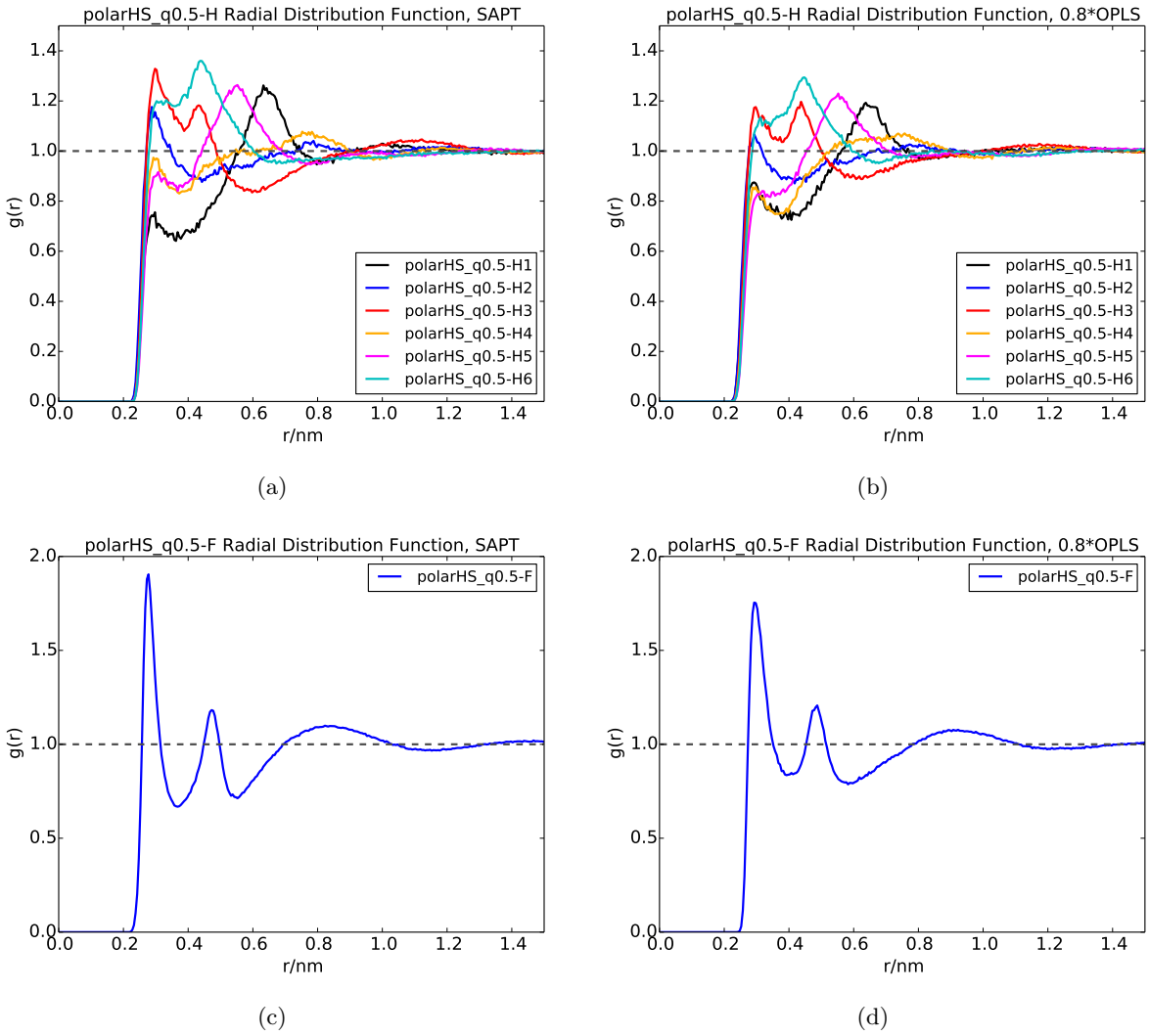

Figure S6: Comparing the 0.8*OPLS and SAPT FF solute-solvent site-site RDFs, polarHS with $q = 0.5$ case. (a) solute-H RDF for SAPT, (b) solute-H RDF for 0.8*OPLS, (c) solute-H RDF for 0.8*OPLS-c, (d) solute-F RDF for SAPT, (e) solute-F RDF for 0.8*OPLS, (f) solute-F RDF for 0.8*OPLS-c.

References

(1) Harris, J. G.; Yung, K. H. Carbon Dioxide's Liquid-Vapor Coexistence Curve and Critical Properties As Predicted by a Simple Molecular Model. *J. Phys. Chem.* **1995**, *99*, 12021–12024.

(2) Rizzo, R. C.; Jorgensen, W. L. OPLS All-Atom Model for Amines: Resolution of the Amine Hydration Problem. *J. Am. Chem. Soc.* **1999**, *121*, 4827–4836.

(3) Yu, K.; McDaniel, J. G.; Schmidt, J. R. Physically Motivated, Robust, ab Initio Force Fields for CO_2 and N_2. *J. Phys. Chem. B* **2011**, *115*, 10054–10063.

(4) Van Vleet, M. J.; Misquitta, A. J.; Stone, A. J.; Schmidt, J. R. Beyond Born-Mayer: Improved Models for Short-Range Repulsion in ab Initio Force Fields. *J. Chem. Theory Comput.* **2016**, *12*, 3851–3870.

(5) Van Vleet, M. J.; Misquitta, A. J.; Schmidt, J. R. New Angles on Standard Force Fields: Toward a General Approach for Treating Atomic-Level Anisotropy. *J. Chem. Theory Comput.* **2018**, *14*, 739–758.

(6) Tillner-Roth, R.; Harms-Watzenberg, F.; Baehr, H. Eine neue Fundamentalgleichung für Ammoniak. *DKV Tagungsbericht* **1993**, *20*, 167–180.

(7) Steinbrecher, T.; Mobley, D. L.; Case, D. A. Nonlinear Scaling Schemes for Lennard-Jones Interactions in Free Energy Calculations. *J. Chem. Phys.* **2007**, *127*, 214108.

(8) Frenkel, D.; Smit, B., *Understanding Molecular Simulations: from Algorithms to Applications*; Academic Press: San Diego, 2002.